Thermal rarefied gas flow investigations through micro/nano backward-facing step: Comparison of DSMC and CFD subject to hybrid slip and jump boundary conditions

Amir-Mehran Mahdavi[1], Nam T.P. Le[1], Ehsan Roohi[1,*], Craig White[2]

1. High Performance Computing (HPC) Laboratory, Department of Mechanical Engineering, Ferdowsi University of Mashhad, P.O. Box 91775-1111, Mashhad, Iran

2. Department of Mechanical and Aerospace Engineering, University of Strathclyde, Glasgow G11XJ, United Kingdom

Abstract

This paper evaluates the suitability of a newly developed hybrid "Langmuir-Maxwell" and "Langmuir-Smoluchowski" slip/jump boundary conditions in the Navier-Stokes-Fourier equations for nano/micro backward-facing step geometry flow which experiences separation and reattachment. Additionally, this paper investigates the effect of different parameters such as step pressure ratio, inflow temperature and wall temperature on the separation zone in the nano/micro step geometry. We chose nitrogen as the working gas and use two DSMC solvers to assess the accuracy of the CFD solutions. DSMC results showed that the increase of the inlet temperatures extends the length of the separation zone and raises the mass flow rate. The change of pressure ratio does not affect the separation length while the increase of the step wall temperature decreases the length of this zone for both CFD and DSMC results. Compared to the DSMC results, the hybrid slip/jump boundary conditions predict better surface pressure, surface gas temperature and slip velocity in the separation zone than the standard Maxwell/Smoluchowski boundary conditions.

Keywords: Nano/micro step**,** DSMC method, hybrid slip/jump boundary conditions, separation zone.

[*] Corresponding author, Tel: + 98 (511) 8805136, Fax: + 98 (511) 8763304, Email: e.roohi@ferdowsi.um.ac.ir

NOMENCLATURE

$\mathbf{I}$	identity tensor	T	temperature, K
$\mathbf{n}$	unit normal vector	T_S	constant temperature, K
$\mathbf{q}$	heat flux, W/m^2	x	Running distance along the wall-3, m
$\mathbf{Q}$	heat flux vector along the surface, W/m^2	α	fraction of coverage α
$\mathbf{S}$	tensor	β	equilibrium constant
$\mathbf{u}$	velocity (m/s)	γ	specific heat ratio
$\mathbf{\Pi}$	stress tensor at the surface, Pa	λ	mean free path, m
$\mathbf{\Pi}_{mc}$	curvature effect term, Pa	μ	viscosity, Pa.s
$\boldsymbol{\tau}$	shear stress, Pa	$\emptyset$	variable of interest e.g. velocity or
A_m	mean area of a site, m^2/mol		temperature
A_S	constant for Sutherland's law,	P	gas density, kg/m^3
	Pa s $K^{-1/2}$	σ_u	tangential momentum accommodation
d	molecular diameter, m		coefficient
D_e	heat of adsorption, J/mol	σ_T	thermal accommodation coefficient
H	height of the channel, m	$\nabla_{\mathbf{n}}$	gradient normal to the boundary surface
Kn	Knudsen number	∇	gradient
L	length of the separation zone, m		
L_C	length of the channel, m	**Subscripts/Superscripts**	
L_1	length of the wall-1, m	in	inlet
N_A	Avogadro number	out	outlet
p	gas pressure at the surface, Pa	w	wall
Pr	Prandtl number	tr	trace
R	specific gas constant, $m^2 s^{-2} K^{-1}$	T	transpose
R_u	universal gas constant, $m^2 s^{-2} K^{-1}$	T_w	
S	height of the channel step, m		

1. Introduction

In the past decades, nano/micro devices have been widely developed and employed in the most of the engineering applications [1]. In this regards, gaseous Nano/micro Electronic Mechanical Systems (MEMS/NEMS) have been developed for the measurement and control in the atomic level. These systems

may include straight nano/micro channels or may contain a series of channels. Numerical simulation of the pressure-driven gas flows in the nano/micro channels is important for understanding of the gas flow behavior. In MEMS/NEMS, fluid mechanics and heat transfer of the gas nano/micro-flows due to nonequilibrium effect such as rarefaction and gas-surface interactions play an important role. Translational nonequilibrium of a rarefied gas flow in nano/micro devices can be characterized by the Knudsen number, *Kn*, that is the ratio of the molecular mean free path, λ, to the characteristic length of the geometry, *l*. If the gas density is relatively high and *Kn* is small, gas flows may be simulated by solving the conventional Navier-Stokes-Fourier (NSF) equations ($Kn \leq 0.001$). When the gas density becomes lower and the gas is rarefied, the gas mean free path becomes large and the nonequilibrium behaviour becomes appreciable. There are fewer collisions between molecules in the flow around the walls. The lack of collisions means the NSF equations become inappropriate in the rarefied regimes indicated by a large Knudsen number. An approach to improve the NSF equations in the range of $0.001 \leq Kn \leq 0.1$, i.e., slip regime, is to use velocity slip and temperature jump boundary conditions. However, when *Kn* rises into the range $0.1 \leq Kn \leq 1$, which is called the transition regime; the NSF equations become inappropriate because the near-equilibrium fluid assumption for flows has broken down. For $Kn > 10$, the molecular density is very low and molecules lack of collisions each other and collisions often occur at the boundary of the geometry. This regime is called as free-molecular regime.

Typical methods used to simulate rarefied gas flows in nano/micro devices in slip regime are the direct simulation Monte Carlo (DSMC) and Computational Fluid Dynamics (CFD).The DSMC method has successfully simulated rarefied gas flows in all the different regimes, but the computational effort is quite expensive especially at lower Kn number flows. A typical CFD method, which solves the NS equations with appropriate surface boundary conditions, may simulate successfully a rarefied gas flow in the continuum regime, up to a *Kn* of 0.1. The computational effort of CFD is much less than the DSMC method, especially for three dimensional flows.

Separation and reattachment are two important features of the internal flows with the change of area. These features have an important effect on the fluid behavior such as mass flow rate and heat transfer characteristic. Backward-facing step is a typical geometry utilized in nano/micro devices. The behavior of step flow is governed by the separation and reattachment.

Some researchers had already considered the gas flows through nano/micro backward-facing step channels. Beskok [2] studied a backward-facing step as the prototype geometry for modeling separated rarefied gas flow. His test case was important to quantify the behavior of rarefied gas flows under adverse pressure gradient and the separation. He investigated the validity and robustness of continuum-based slip models for $Kn < 0.1$, by comparing the CFD simulation results obtained with Maxwell's first-order and the second order slip models against his DSMC data. The Langmuir slip developed in Ref. [3] combined with

the NS equations was proposed and implemented for backward-facing step gas flow in the slip regime by Choi *et al*. [4].A characteristic-based split Navier-Stokes FEM solver was used for the simulations of rarefied gas flow through a backward-facing step duct in THE slip regime by Celik and Edis [5]. The second-order slip-velocity and temperature-jump boundary conditions suggested by Beskok [2] were applied on the duct walls. Rached and Daher [6] numerically investigated the incompressible rarefied gas microflow and heat transfer in backward-facing step microchannel in slip regime. A control-volume based numerical method is used to solve the NSF equations with the velocity-slip and temperature-jump boundary conditions at the walls. Their simulation results provided numerical data for incompressible flows over a backward-facing step. Control of separated flow past a backward-facing step in a microchannel was studied by Baysal *et al.* [7] based on the NSF equations with slip/jump boundary condition in the range $0.01 < Kn < 0.1$. Xue and Chen [8] simulated micro-backward-facing step flows in both slip and transition flow regimes by the DSMC method. Their results showed that the phenomena of flow separation, recirculation, and reattachment will disappear as *Kn* number exceeds 0.1. A significant jump of pressure and velocity behind the step was observed in the transition flow regime. The compressibility had significant effect on flow characteristics in the slip regime but would be negated by the rarefaction in the transition flow regime [8]. Xue *et al.* [9] figured out that the stability of the vortex behind the step relies on the magnitudes of mean and thermal velocities in the region, which are closely related to the *Kn* number, local temperature, and driving pressure ratio. A highly intensified pressure and velocity region behind the step is identified in the transition flow regime [9]. Kursun and Kapat [10] used IP-DSMC to simulate the gas flow through the backward-facing step microchannel with various Reynolds number Re of 0.03 to 0.64, Mach number (*Ma*) of 0.013 to 0.083, and *Kn* of 0.24 to 4.81. For these parameter values, no separation region is observed, and the high heat flux associated with reattachment was also absent. Schafer *et al.* [11] researched the separation zone of a backward-facing step in macro scale. They also pointed out that the backward-facing step flow is extremely sensitive to numerical errors and the choice of the boundary conditions at the inlet. Bao *et al.* [12] surveyed the microscale backward-facing step flow in transition regime with CFD solving the Burnett equations. These equations are also limited by very high *Kn*. Darbandi and Roohi [13] used DSMC method to study the effect of *Kn* number for nano/micro backward-facing steps. They concluded that the change of *Kn* number affects on the step flow behavior and the separation zone.

Although there were papers considering rarefied gas flow through backward-facing step in nano/micro scales, our literature survey show that mass flow rate and heat transfer behavior of step flow has not been discussed in details in the literature. Moreover, the effects of the separation zone on the fluid and thermal behavior of nano/micro step has not completely understood. In addition to the above topics, the suitability of a hybrid-type slip boundary conditions for the slip regime is another focus of the current

work. In this paper, we use both DSMC and CFD to model the behavior of the pressure-driven rarefied gas flows through 2-D backward-facing step geometry in the range $0.01 \leq Kn \leq 0.1$. CFD, in particular the NSF equations, combined with newly developed slip/jump boundary conditions, are investigated for the first time for flows with separation and reattachment. Input simulated parameters are also changed to investigate their effects on the separation region and its length. DSMC simulations are run with the DSMC code developed and validated by Roohi and co-workers [13-18] and *dsmcFoamStrath* [19-20] developed in the framework of open source CFD toolbox, OpenFOAM [21]. CFD simulations are run using the *rhoCentralFoam* solver in the OpenFOAM. In this solver, the NSF equations were numerically solved with the high-resolution central scheme described by Greenshields *et al.* [22]. The results presented in Ref. [22] indicated that this central scheme is competitive with the best method previously published, and is simple and well-suited to a collocated, polyhedral finite volume framework.

The accuracy of the NSF simulations depends on the surface boundary conditions applied. The Maxwell slip velocity [23] and the Smoluchowski temperature jump [24] boundary conditions for CFD are revisited in the present work. Recently, Le *et al*. [25] proposed the Langmuir-Maxwell and Langmuir-Smoluchowski boundary conditions, so-called "hybrid boundary conditions", for rarefied gas simulation by combining the Langmuir adsorption isotherm and kinetic theory. These hybrid conditions are investigated in the present study for a flow with separation and reattachments.

2. Direct Simulation Monte-Carlo (DSMC)

For decades, DSMC technique has been regarded as a powerful numerical method for studying rarefied gas dynamics problems. The DSMC technique uses a finite set of model particles denoted by their positions and velocities which move and collide in a computational domain to perform a stochastic simulation of the real molecular gas dynamics. The basic concept of the method is built on a discretization in time and space of the real gas dynamics process and splitting the motion into two successive stages of free molecular motion and binary intermolecular collisions within the grid cells in each time step. A rigorous mathematical proof of the method convergence for a large enough number of particles in cells to the Boltzmann equations was given by Wagner [26].

DSMC is a direct simulation algorithm for rarefied gas flow based on the kinetic theory. It simulates gas flow as a collision of discrete particles with various position, velocities, and energies. In DSMC, each simulated particle represents a large number of real molecules with the same properties. During the simulation, the molecular motions and intermolecular collisions are performed over small time steps which are smaller than the mean collision time. The macroscopic quantities such as flow velocities, densities, and temperatures are calculated through sampling the microscopic quantities of all the particles

in the computational domain. Typical applications of the DSMC algorithms were presented in Refs. [27-28].

3. Computational Fluid Dynamics (CFD)

The governing equations, in particular NSF equations, solved by the CFD method are based on the assumptions that the fluid consists of a continuum environment where the perfect gas law applies, and the only forces are due to pressure, viscous effects and body forces. In our CFD solver, i.e., *rhoCentralFoam*, the governing equations are numerically solved by the finite volume method, see Ref. [22]. Various nonequilibrium slip/jump boundary conditions are implemented into our NSF solver to investigate the flow behaviour in the nano/micro backward-facing step geometry. In the present work the Maxwell, Smoluchowski, Langmuir-Maxwell and Langmuir-Smoluchowski (so-called hybrid boundary condition) are selected to capture the flow behaviour in the step geometry.

The Maxwell slip boundary condition including the effect of thermal creep, can be expressed in vector form as [23]:

$$\mathbf{u} = -\left(\frac{2-\sigma_u}{\sigma_u}\right)\frac{\lambda}{\mu}\boldsymbol{\tau} - \frac{3}{4}\frac{\Pr(\gamma-1)}{\gamma p}\mathbf{q} + \mathbf{u}_w, \tag{1}$$

where the tangential shear stress is $\boldsymbol{\tau} = -\mathbf{S}\cdot(\mathbf{n}\cdot\boldsymbol{\Pi})$ and the heat flux is $\mathbf{q} = \mathbf{Q}\cdot\mathbf{S}$ at the surface; the tensor $\mathbf{S} = \mathbf{I} - \mathbf{nn}$ removes normal components of any non-scalar field, e.g. velocity, so that slip only occurs in the direction tangential to the surface; $\mathbf{n}$ is the unit normal vector defined as positive in the direction pointing out of the flow domain. The tangential momentum accommodation coefficient determines the proportion of molecules reflected from the surface specularly (equal to $1-\sigma_u$) or diffusely (equal to σ_u), and $0 \le \sigma_u \le 1$. Substituting $\boldsymbol{\tau} = -\mathbf{S}\cdot(\mathbf{n}\cdot\boldsymbol{\Pi})$ and $\boldsymbol{\Pi} = \mu\nabla\mathbf{u} + \boldsymbol{\Pi}_{mc}$ with $\boldsymbol{\Pi}_{mc} = \mu(\nabla\mathbf{u})^T - \left(\frac{2}{3}\right)\mathbf{I}\mathrm{tr}(\nabla\mathbf{u})$ into Eq. (1), and noting that $\mathbf{S}\cdot\nabla_{\mathbf{n}}\phi \equiv \nabla_{\mathbf{n}}(\mathbf{S}\cdot\phi)$, Eq.(1) becomes:

$$\mathbf{u} + \left(\frac{2-\sigma_u}{\sigma_u}\right)\lambda\nabla_{\mathbf{n}}(\mathbf{S}\cdot\mathbf{u}) = \mathbf{u}_w - \left(\frac{2-\sigma_u}{\sigma_u}\right)\frac{\lambda}{\mu}\mathbf{S}\cdot(\mathbf{n}\cdot\boldsymbol{\Pi}_{mc}) - \frac{3}{4}\frac{\mu}{\rho}\frac{\mathbf{S}\cdot\nabla T}{T}. \tag{2}$$

The right hand side of Eq. (2) contains 3 terms that are associated with (in order): the surface velocity, the so-called curvature effect [23], and thermal creep. The Maxwellian mean free path is defined as follows:

$$\lambda = \frac{\mu}{\rho}\sqrt{\frac{\pi}{2RT}}. \tag{3}$$

The viscosity μ is computed by Sutherland's law:

$$\mu = A_S \frac{T^{1.5}}{T + T_S}, \tag{4}$$

where A_S = 1.41 x 10^{-6} Pa s $K^{-1/2}$ and T_S = 111 K for nitrogen [25].

Experimental observations show that the temperature of a rarefied gas at a surface is not equal to the wall temperature, T_w. This difference is called the "temperature jump" and is driven by the heat flux normal to the surface. The Smoluchowski boundary condition can be written [24]:

$$T + \frac{2-\sigma_T}{\sigma_T}\frac{2\gamma}{(\gamma+1)\mathrm{Pr}}\lambda\nabla_{\mathbf{n}}T = T_w, \tag{5}$$

where σ_T is thermal accommodation coefficient $(0 \le \sigma_T \le 1)$. Perfect energy exchange between the gas and the solid surface corresponds to σ_T= 1, and no energy exchange to σ_T= 0.

The hybrid conditions such as the Langmuir-Maxwell (LM) and Langmuir-Smoluchowski (LS) conditions were proposed by Le *et al.* [25] by inserting the Langmuir adsorption isotherm [3, 29] into the Maxwell and Smoluchowski (MS) equations. They assumed that only diffuse reflection and perfect energy exchange are taken into account for developing these hybrid slip/jump conditions (i.e. $\sigma_u = \sigma_T$= 1.0), in which the molecules adsorbed at the surface are considered as diffusely reflected. The molecules adsorbed that are determined by the fraction of coverage α $(0 \le \alpha \le 1)$, only contribute to the part of the total fluid shear stress at the surface due to the approaching molecules. The temperature of these emitted molecules is equal to the surface temperature ($T = T_w$). The hybrid slip and jump conditions were presented in Ref. [25] as follows:

$$\mathbf{u} + \left(\frac{1}{1-\alpha}\right)\lambda\nabla_{\mathbf{n}}(\mathbf{S}\cdot\mathbf{u}) = \mathbf{u}_w - \left(\frac{1}{1-\alpha}\right)\frac{\lambda}{\mu}\mathbf{S}\cdot(\mathbf{n}\cdot\boldsymbol{\Pi}_{\mathrm{mc}}) - \frac{3}{4}\frac{\mu}{\rho}\frac{\mathbf{S}\cdot\nabla T}{T}, \tag{6}$$

which the right hand side of the hybrid slip condition also contains three terms that are associated with (in order): the surface velocity, the so-called curvature effect [23], and thermal creep. The hybrid jump condition is

$$T + \frac{1}{1-\alpha}\frac{2\gamma}{(\gamma+1)\mathrm{Pr}}\lambda\nabla_{\mathbf{n}}T = T_w. \tag{7}$$

The fraction of coverage α is computed by the Langmuir adsorption isotherm [3, 29]. For monatomic gas

$$\alpha = \frac{\beta p}{1+\beta p}, \tag{8}$$

and for diatomic gas

$$\alpha = \frac{\sqrt{\beta p}}{1+\sqrt{\beta p}}, \tag{9}$$

where β is an equilibrium constant relating to the surface temperature, given by:

$$\beta = \frac{A_m \lambda}{R_u T_w} \exp\left(\frac{D_e}{R_u T_w}\right), \tag{10}$$

where A_m is either measured or calculated approximately by $N_A \pi d^2/4$ for gases [3, 29]; d is Covalent diameter of the molecule: for nitrogen gas d = 0.142 nm [25]; D_e is the measured value of the heat of adsorption (J/mol): for argon and nitrogen gases D_e= 5255 (J/mol) given in references [3, 29]. These conditions were implemented into the solver *rhoCentralFoam* in OpenFOAM for simulating rarefied gas flows [25, 30].

These new hybrid conditions go some way towards addressing the problem of the values of free coefficients (σ_u and σ_T) in the Maxwell/Smoluchowski slip/jump boundary conditions. The fraction α is not constant along the solid surface for all the CFD simulation cases. This is more realistic than applying constant values of σ_u and σ_T along the solid surface, which is usually done in CFD simulations. These new hybrid conditions predict precisely surface pressure for high speed rarefied gas flows, and they evaluate, however, higher slip velocity and temperature jump than MS conditions [25]. In this work, we would like to extend these boundary conditions to capture the behaviour of the low speed microscale rarefied gas flows.

4. Numerical setup

A typical numerical setup for a CFD simulation for the pressure-driven rarefied gas flow through a nano/micro backward-facing step channel is presented in Fig. 1. In CFD simulations, various nonequilibrium boundary conditions are applied on the walls of the channel for the flow variables (T, $\mathbf{u}$). The boundary condition for the pressure p at the walls is zero normal gradient condition. At the inflow boundary, the inlet conditions for (p, T) were maintained throughout the computational process and zero normal gradient condition is applied for the inflow boundary condition of velocity. At the outflow boundary, the outlet pressure is specified and the normal gradients of the flow variables (T, $\mathbf{u}$) vanish at this boundary. The boundary conditions for DSMC simulations include explicit values for p_{in}, T_{in} and p_{out}. Boundary conditions for $\mathbf{u}_{in}$, $\mathbf{u}_{out}$ and T_{out} are implicitly applied in the DSMC scheme, as detailed in Ref. [31]. In the DSMC, the number of Particles Per Cell (PPC) are determined by the user. Evidently, the increase of PPC improves the accuracy of the simulations but it increases the computational costs.

Different PPC were independently studied for DSMC cases in the present work. From obtained simulation results with various PPC, we choose PPC = 16 for DSMC results reported in the current work.

The input parameters, dimensions of the nano/micro step channel for both DSMC and CFD simulations are presented in Tables 1 and 2. Mesh independence analysis was conducted for all DSMC and CFD simulations and only final mesh sizes of rectangular mesh are also presented in Table 2. The size of considered step geometry is at the nano scale.

5. Numerical results and discussions

Numerical CFD and DSMC results of all simulations will be presented in this section. We present all numerical results on the wall-3 of the step channel only in the streamwise direction because the separation zone locates over this wall. The pressure values, p, are normalized by the inlet pressure, p_{in}. CFD simulations are run with various boundary conditions such as Maxwell/Smoluchowski (MS) and hybrid slip/jump boundary conditions (LMS). The values of tangential momentum accommodation coefficient, $\sigma_u = 1.0$ and thermal accommodation coefficient, $\sigma_T = 1.0$ are used for both CFD and DSMC runs. DSMC code used in Ref. [13] was employed for DSMC simulations in cases of various inlet temperatures, pressure ratios and the wall temperatures.

5.1 Various inlet temperature cases

Three various inlet temperatures T_{in} = 300 K, 500 K and 700 K are set for both CFD and DSMC runs. Figure 2 shows the pressure variation along wall-3. At the tip of wall-3, the surface pressures raise up to a peak normalized pressure and thereafter gradually decreases along the wall-3. For the case T_{in} = 300 K, the hybrid boundary conditions predict better surface pressure than the MS boundary conditions in comparison with the DSMC results, as seen in Fig. 2-a. For cases T_{in} = 500 K and 700 K, Figs. 2-b and 2-c, there are large differences between the CFD and DSMC surface pressure in the locations 25.6 nm < x < 50 nm in which the CFD overpredicts the surface pressure. For the case T_{in} = 500 K, the obtained results show the peak normalized surface pressures of 0.61 for the MS conditions, 0.60 for LMS conditions and *0.575* for DSMC; and 0.6, 0.59 and 0.55 respectively for the case T_{in} = 700 K. Past these peak points, the surface pressures gradually decrease and solution become close together in the range 50 nm < x < 85.47 nm. Surface pressures decrease in the separation zone when T_{in} increases, in which DSMC surface pressures significantly decrease.

For surface gas temperature shown in Fig. 3-a, both DSMC and CFD results are close together in the case T_{in} = 300 K. For two remaining cases, the surface gas temperatures increase to the peak temperature and then gradually decrease along the wall-3. The peak temperatures in the case T_{in} = 500 K are 302 K for the MS conditions, 307 K for the hybrid conditions, and 307 K for DSMC as seen in Figs.

3-b; and 304 K, 312 K, and 315 K, respectively for the case T_{in} = 700 K, as seen Fig. 3-c. Both of cases, the predictions of hybrid conditions for the gas surface temperature are closer to the DSMC data than those of the MS conditions.

Slip velocities on the wall-3 consist of negative and positive components. Negative ones represent the separation zone, and the distance, where indicates the negative slip velocities, is defined as the length of the separation zone, L. It is seen that in this zone that the hybrid slip/jump boundary conditions give better slip velocities than MS conditions in comparison with the DSMC data. Beyond this zone, the slip velocities obtained with the MS conditions are closer to the DSMC data than the hybrid conditions for the cases T_{in} = 300 K and 500 K, as seen in Figs. 4-a and 4-b. In the distance 60 nm < x < 80 nm, Fig. 4-c, the hybrid boundary conditions produce slip velocity closer to those of the DSMC than the MS conditions for the case T_{in} = 700 K. As seen in Figs. 4 and 5, DSMC results showed that the increase of the inlet temperature at fixed Kn_{in} will increase the velocity magnitude in the separation zone and extend the length of this zone. The lengths, L, in DSMC simulations are 13.9 nm for the case T_{in} = 300 K, 17.9 nm for the case T_{in} = 500 K, and 21.9 nm for the case T_{in} = 700K. *Both CFD simulation results using LMS and MS conditions are nearly constant values of 12.9 nm and 12.4 nm, respectively.* In DSMC, the heating gas molecules have more energy to jump over the circulation region resulting in increasing the length of the separation region. Velocity magnitudes of DSMC results are highest in the separation zone. Beyond this zone, the slip velocity magnitudes of the hybrid condition results are highest and those of the MS conditions are lowest along the wall-3.

5.2 Various pressure ratio

In this section, the outlet pressure is changed with various values to investigate its effect on the gas flow behavior. Firstly, DSMC simulations were run with various pressure ratios (PR) as 1.5, 2.5, 3, 4, 5, 6 and 7. The DSMC results show that the change of the pressure ratio will affect on the mass flow rate, as shown in Fig. 6. It is seen that the mass flow directly varies with the pressure ratio in the pressure driven channel. However, when the pressure ratio is greater than 4, there is not any visible effect on the mass flow. It is due to the fact that the gas flow approaches the choking condition at higher pressure ratio. According to this DSMC result, we just did the comparison between CFD and DSMC simulations for various pressure ratios of 1.5, 2.5, 3 and 4. At the tip of the wall-3, surface pressures reach to peak normalize values and thereafter gradually decrease along the wall-3. The predictions for surface pressures with the hybrid conditions are better than those of the MS conditions in comparison with the DSMC data for all cases, as seen in Fig. 7. Surface pressure decreases when the pressure ratio increases. For the slip velocity, the hybrid conditions give better results than the MS boundary conditions in the recirculation region comparing with the DSMC data, in which the hybrid boundary condition results give the best

agreement with the DSMC data for the case PR = 1.5, as seen in Fig. 8-a. Beyond this region, the predictions for slip velocity with the MS boundary conditions are better than that of the hybrid conditions in comparing with the DSMC data for all cases, as seen in Fig. 8. The magnitudes of the peak slip velocity in the recirculation zone raise up when the PR increases from 1.5 to 2.5, while those do not change for the remaining cases, as seen in Fig. 8. Beyond the separation zone, the magnitudes of slip velocity also raise up when the pressure ratio increases.

The variation of the separated length, L, is presented in Fig. 9. There was a slightly decrease of L in DSMC simulations from 13.4 nm to 13.1 nm when increasing the pressure ratio. The simulation results using hybrid conditions (LMS) show that the separation length raises from 12.6 nm to 13.6 nm when the pressure ratio increases from 1.5 to 2.5. The L is nearly constant value of 13.6 nm when the pressure ratio is greater than 2.5. The simulation results using MS conditions present a jump of L from 10.1 nm to 11.7 nm between the pressure ratios of 2.5 and 3. In overall, the simulation results using hybrid conditions are close to DSMC data.

5.3 Various wall temperatures

In this section, we change the temperatures of the wall-2 and 3 which are located near the separation zone. We set two different wall temperatures T_w = 500 K and 700 K to investigate the effect of the increase of the wall temperature on the gas flow behavior in the separation zone. Similar to the cases with various T_{in} and PR, surface pressures increase to peak values at the tip of the wall-3 and then gradually decrease along the wall-3. The peak normalized pressure values are 0.65 for the MS conditions, 0.65 for DSMC and 0.645 for the hybrid conditions for the case T_w = 500 K, as shown in Fig. 10-a; and 0.69, 0.685 and 0.68 respectively for the case T_w = 700 K, as seen in Fig. 10-b. The hybrid boundary conditions predict more accurate surface pressure than the MS boundary conditions comparing with the DSMC data for both cases, *even in separate region. This is caused by the increase of the wall temperature that affects significantly the computation of the values α and β in Eqs. (9) and (10), respectively*. Surface pressures also increase along the wall-3 when T_w increases. Surface gas temperatures reach a peak temperature at the tip point and then gradually decrease toward the location x = 40 nm and slightly increases along the rest of the wall-3. The peak temperatures are 497.5 for the MS conditions, 497.5 K for DSMC, and 493 K for the hybrid conditions for the case T_w = 500 K shown in Fig. 11-a; and 692 K, 690 K and 682 K respectively for the case T_w = 700 K, as seen in Fig. 11-b. The MS boundary conditions give a suitable agreement with DSMC data of the surface gas temperature, while the hybrid boundary conditions under-predict that temperature for both cases. In the separation zone, when the T_w increases the magnitudes of the slip velocities reduce, while beyond this zone the magnitudes of slip velocities increase, as seen in Fig. 12. The hybrid boundary conditions give better agreement with the DSMC data for slip velocity in the separation region. Beyond this region, the MS conditions give the best

agreement with the DSMC data for the slip velocity while the hybrid boundary conditions overpredict that velocity for both cases.

The lengths of the separation zone, L, for the case T_w = 300K are 13.9 nm for DSMC, 12.9 nm for the hybrid LMS conditions and 12.4 nm for the MS boundary conditions; and 9.9 nm, 8.9 nm and 6.9 nm, respectively for the case T_w = 500 K; and 7.9 nm, 6.9 nm and 4.4 nm, respectively for the case T_w = 700 K; as seen in Fig. 13. The separation lengths of both DSMC and CFD simulations decrease when the wall temperature increases. The simulation results using hybrid LMS conditions are closer to DSMC results than those of the MS conditions.

5.4 Simulation cases with Kn_{in} = 0.05 and 0.1

In this section, DSMC simulations were run with *dsmcFoamStrath* [20] and DSMC code used in Ref. [13]. Three cases with Kn_{in} = 0.05 and 0.1 are simulated in which two cases with Kn_{in} = 0.1 are carried out for two different step microchannels. The input parameters, dimensions of microchannel of three cases, DSMC solvers and final mesh sizes are presented in Table 3.

The case 1, Kn_{in} = 0.05, is run with *dsmcFoamStrath* [20]. For the surface pressures in the range 1.81 μm ≤ x ≤ 2.6 μm, as shown in Fig. 14, the MS boundary conditions give suitable agreement with the DSMC data, and all of them are close together in the location 2.6 μm ≤ x ≤ 5.6 μm. Both DSMC and CFD captured the separation zone shown in Fig. 15. The slip velocities in the separation zone are also close together. Beyond this zone, the slip velocity obtained with the MS boundary conditions give better agreement with that of DSMC data. The lengths of the separation for DSMC and CFD data are equal to 0.3 μm.

In both cases 2 and 3 with Kn_{in} = 0.1, the results of the MS conditions are in better agreement than those of the hybrid conditions with the DSMC data for both of the surface pressure and slip velocity over the wall-3, as seen in Figs. 16, 17, 18 and 19. It is seen that when the Kn_{in} increases, the length of the recirculation zone decreases. This can be explained as Kn_{in} increases the flow is more viscous and become closer to the creeping flow condition. Creeping flow does not experience the separation due to the attachment to the walls that the viscosity enforces.

It is mentioned that both cases with Kn_{in} = 0.1, which are run by two different DSMC solvers, show the recirculation zone while CFD solver does not, as seen Figs. 17 and 19. It is due to the point that flow experiences a high degree of non-equilibrium in the wake region, which could not be captured by the NS equations. In the test case 2 with Kn_{in} = 0.1, the separation zone of DSMC result is very small that was represented by one point of negative slip velocity, while the length of this zone of the test case 3 is around 0.4 μm.

6. Conclusions

Gas flow behaviours in the nano/micro backward-facing step geometry have been studied using both DSMC and CFD techniques. The effects of input parameters on the separation zone had been considered in details. For 0.01 <Kn_{in}< 0.05 and corresponding to the cases of various T_{in}, pressure ratios and T_w, the hybrid "Langmuir-Maxwell" and "Langmuir-Smoluchowski" slip/jump (LMS) boundary conditions predict more accurate surface pressure than the "Maxwell/Smoluchowski" (MS) boundary conditions in comparison with the DSMC data. For the slip velocity, the LMS conditions give good agreements with the DSMC data in the separation zone, while the MS conditions predict better slip velocities than LMS conditions in comparing the DSMC data beyond the separation zone. The LMS boundary conditions predict surface gas temperature better than the MS boundary conditions in comparison with DSMC data when T_{in} increases, while the MS conditions predict those better than the LMS conditions when T_w increases. The DSMC results obtained show that the mass flow rate does not change if pressure ratio becomes greater than 4. The increase of T_{in} results in the extension of the length of the separation zone in DSMC simulations and this length is nearly constant values for CFD simulations. An increase in T_{wall} reduce the length of the separation zone for both DSMC and CFD. This length has no much sensibility with the increase of the pressure ratio. For the cases Kn_{in} = 0.05 and 0.1, the MS boundary conditions give good agreements for the surface pressure and slip velocity in comparison with the DSMC data. The length of the separation zone decreases once Kn_{in} increased. Finally, CFD solutions with different slip/jump boundary conditions could not capture the separation region at Kn_{in}=0.1 due to increased non-equilibrium effects.

Acknowledgements

The authors from Ferdowsi University of Mashhad would like to acknowledge the financial supports provided by "Iranian Elite Foundation" under grant No. 100720.

References

1.Ho C. M. Tai Y. C., Micro-Electro-Mechanical Systems- and Fluid Flows, *Annu. Rev. Fluid Mechanics*, Vol. 30, 579–612, 1998.

2. Beskok A., Validation of a new velocity-slip model for separated gas microflows. *Numerical Heat Transfer*, Part B, 40: 451-471, 2001

3. Myong, R. S. 2004. Gaseous slip models based on the Langmuir adsorption isotherm. *Physics of Fluids 16*, 104 17.

4. Choi, H., Lee, D. H., Lee, D., Complex microscale flow simulations using Langmuir slip condition, *Numerical Heat Transfer*, Part A, Vol. 48, 407 – 425, 2005.

5. Celik, B., Edis, F.O., Computational Investigation of Micro Backward-Facing Step Duct Flow in Slip Regime, *Nanoscale and Microscale Thermophysical Engineering*, Vol. 11, 319-331, 2007.

6. Rached, J., Daher, N., Numerical prediction of slip flow and heat transfer in microchannels, *Proceedings of the 6th Annual Engineering Students Conference - American University of Beirut*, Lebanon, 109 – 114, 2007

7.Baysal, O., Erbas, N. and Koklu, M, Control of separated flow past a backward-facing step in a microchannel, *Microfluidics and Nanofluidics*, Vol. 1, 86 – 92, 2004.

8.Xue, H., Chen, S.,DSMC simulation of microscale backward-facing step flow, *Microscale Thermophysical Engineering*, Vol. 7, 69-86, 2003.

9.Xue, H., Xu, B., Wei, Y., Wu, J., Unique behaviours of a backward-facing step flow at microscale, *Numerical Heat Transfer*, Part A, Vol. 47, 251-268, 2005.

10. Kursun, U., Kapat, J.S., Modeling of Microscale Gas Flows in Transition Regime Part I: Flow over Backward-facing Steps, *Nanoscale and Microscale Thermophysical Engineering*, Vol. 11, 15-30, 2007.

11.Schafer, F., Breuer, M., Durst, F., The dynamics of the transitional flow over a backward-facing step. *Journal of Fluid Mechanics*, Vol. 623, 85-119, 2009.

12. Bao F. and Lin J.Z., Continuum Simulation of the Microscale Backward-Facing Step Flow in a Transition Regime, *Numerical Heat Transfer*, Part A, 59: 616–632, 2011.

13. Darbandi, M., Roohi, E., DSMC Simulation of subsonic flow through nanochannels and micro/nano backward-facing step, *Int. Communications Heat Mass Transfer* Vol. 38, 1443-1448, 2011.

14. Akhlaghi, H., Balaj, M., Roohi, E., DSMC investigation of Mixed Supersonic-Subsonic Flow through Micro/Nano Channels, Physica Scripta, Vol. 88, 015401,2013.

15. Mohammadzadeh, A., Roohi, E., Niazmand, H., A Parallel DSMC Investigation of Monatomic/Diatomic Gas Flows in Micro/Nano Cavity, *Numerical Heat Transfer, Part A: Applications*, Vol. 63(4), 305-325, 2013.

16. Mohammadzadeh, A., Roohi, E., Niazmand, H., Stefanov, S., Myong, R.S., Detailed Investigation of Thermal and Hydrodynamic Behavior in Micro/Nano Cavity Using DSMC, Physical Review E, Vol. 85, 056305, 2012.

17. Akhlaghi, H., Roohi, E., Mass Flow Rate Prediction of Thermal-Pressure-Driven Gas Flows Through Micro-/Nanoscale Channels, Continuum Mechanics and Thermodynamics, DOI: 10.1007/s00161-013-0290-0, In press.

18. Amiri, A., Roohi, E., Niazmand, H., Stefanov, S., DSMC Simulation of Low Knudsen Micro/Nano Flows using Small Number of Particles per Cells, ASME J. Heat Transfer, Vol. 135(10), 101008, 2013.

19. Scanlon, T., Roohi, E., White, C., Darbandi, M., Reese, J., An Open Source, Parallel DSMC Code for Rarefied Gas Flows in Arbitrary Geometries, *Computers and Fluids*, Vol. 39, 2010, pp. 2078-2089.

20. White, C., Borg, M.K., Scanlon, T., Reese, J. M., A DSMC Investigation of Gas Flows in Micro-Channels With Bends, Computers & Fluids, Vol. 71, 2012, 261–271.
21. OpenFOAM Foundation, http://www.openfoam.org, 2013.
22. Greenshields, C. J., Weller, H. G.,Gasparini, L., Reese, J. M., Non-oscillatory central schemes for high speed viscous flows, *Int. J. Numerical Methods Fluids*, Vol. 23, pp. 1–21, 2010.
23. Maxwell, J. C., On stresses in rarefied gases arising from inequalities of temperature, *Philosophical Transactions of the Royal Society*, Part 1, Vol. 170, pp. 231–256, 1879.
24. Smoluchowski, M. von, Uberwarmeleitung in verdunntengasen, *Annalen der Physik und Chemie*, Vol. 64, pp. 101–130, 1898.
25. Le**,** N. T. P., White, C., Reese, J. M., Myong, R. S., Langmuir-Maxwell and Langmuir-Smoluchowski boundary conditions for thermal gas flow simulations in hypersonic aerodynamics, *Int. J. Heat Mass Transfer,* Vol. 55, 5032 – 5043, 2012.
26. Wagner W., A convergence proof for Bird's direct simulation Monte Carlo method for the Boltzmann equation, *J. Statistical Physics*, Vol. 66, 1011-1044, 1992.
27. Marston, A.J., Daun, K.J., Collins, M.R. Geometric optimization of radiant enclosures containing specularly-reflecting surfaces through quasi-Monte Carlo simulation, Numerical heat transfer; Part A: Applications, 59 (2), pp. 81-97, 2011.
28. Roesle, M. ,Good, P. , Coskun, V. Steinfeld, A. Analysis of conduction heat loss from a parabolic trough solar receiver with active vacuum by direct simulation Monte Carlo, Numerical heat transfer; PartA: Applications, 62 (5), pp. 432-444, 2012.
29. Bhattacharya, D.K., and Eu, B.C., Nonlinear transport processes and fluid dynamics: effects of thermo-viscous coupling and nonlinear transport coefficients on plane Couette flow of Lennard-Jones fluids, *Physical Review A*, Vol. 35, 821 – 836, 1987.
30. Le, N. T. P., Greenshields, C. J., Reese, J. M., Evaluation of nonequilibrium boundary condition in simulating hypersonic gas flows, *Progress in Flight Physics*, Vol. 3,217 – 230, 2012.
31. Akhlaghi, H., Roohi, E., Stefanov, S., A New Iterative Wall Heat Flux Specifying Technique in DSMC for Heating/Cooling Simulation of MEMS/NEMS, *Int. J. Thermal Science*, Vol. 56, 111-125, 2012

Table 1: Input parameters and the dimensions of step nano/micro channels for both DSMC and CFD cases, $0.01 < Kn_{in} < 0.05$.

Case	various T_{in}	various pressure ratio	various T_w at the walls 2 and 3
Inlet temperature T_{in} (K)	300; 500; 700	300	300
Inlet pressure p_{in} (MPa)	31.077290	31.077290	31.077290
Kn_{in} (based on the channel height, H)	0.01; 0.025; 0.034	0.01	0.01
T_{w} for walls 1 and 4 (K)	300	300	300
T_{w} for walls 2 and 3 (K)	300	300	300; 500; 700
Pressure ratio $p_{\text{in}}/p_{\text{out}}$	2	1.5; 2; 3; 4	2
Working gas	Nitrogen	Nitrogen	Nitrogen

Table 2: Dimensions of step nano/micro channels and final mesh sizes for both DSMC and CFD cases, $0.01 < Kn_{in} < 0.05$.

L_C (nm)	85.47
H (nm)	0.2 L
S (nm)	0.1 L
L_1 (nm)	0.3 L
Final number of elements for blocks I; II; III in directions (x, y)	(60×60; 140×60; 140×60)

Table 3: Input parameters, the dimensions of step nano/micro channels, final mesh size and DSMC code for both DSMC and CFD test cases, Kn_{in} = 0.05 and 0.1.

Case	Case 1	Case 2	Case 3
P_{in} (Pa)	150735.8	75397.3	53222.97
Kn_{in} (based on the channel height, H)	0.05	0.1	0.1
Pressure ratio $p_{\text{in}}/p_{\text{out}}$	2.32		2
T_{in} (K)	330		300
T_w (K)	300		300
L_C (μm)	5.61		5
H (μm)	1.0		1.0
S (μm)	0.5		0.5
L_1 (μm)	1.81		1.5
Working gas	Nitrogen		Nitrogen
Final number of elements for blocks I; II; III in directions (x, y)	(61×30; 244×30; 244×30)		(30×30; 70×30; 70×30)
DSMC code	*dsmcFoamStrath* [20]		DSMC solver in [13]

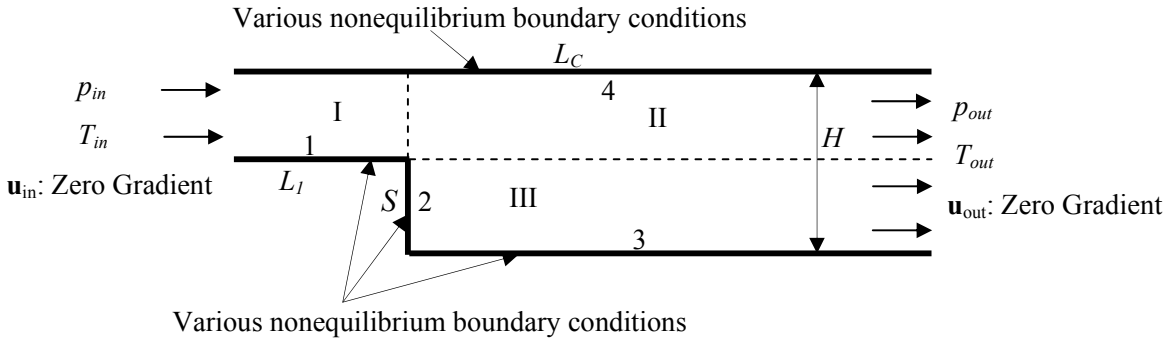

Figure 1: Typically numerical setup for CFD test cases.

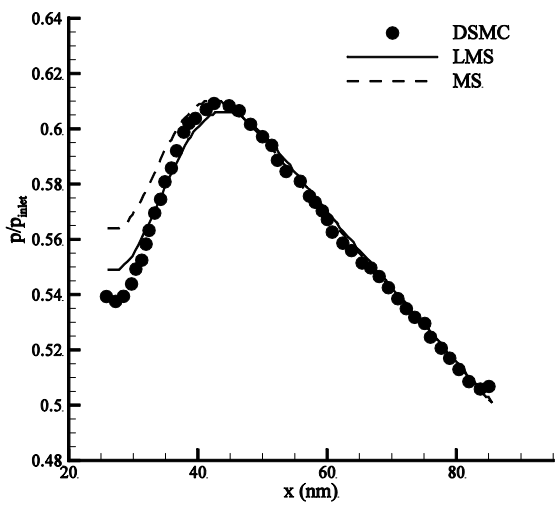

a) T_{in} = 300 K.

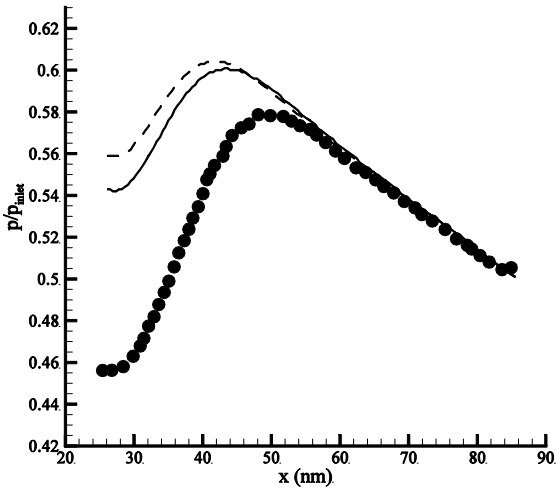

b) T_{in} = 500 K.

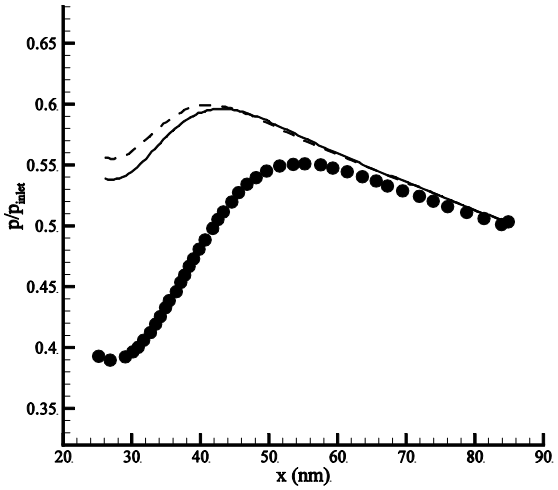

c) T_{in} = 700 K.

Figure 2: Pressure distribution on the wall-3 with various T_{in}.

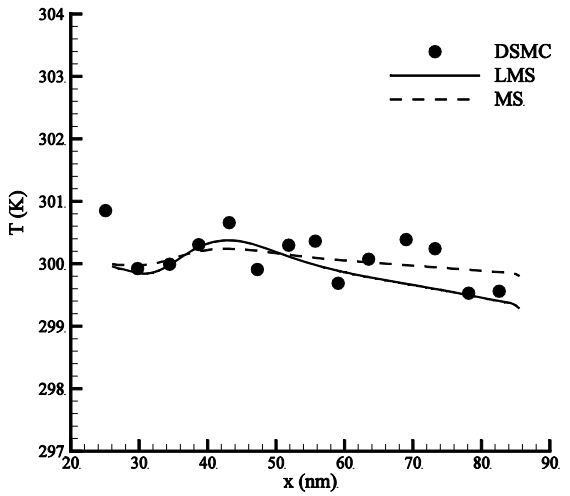

a) T_{in} = 300 K.

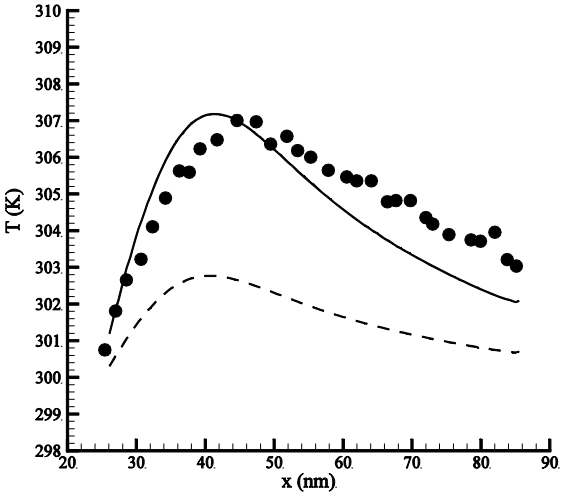

b) T_{in} = 500 K.

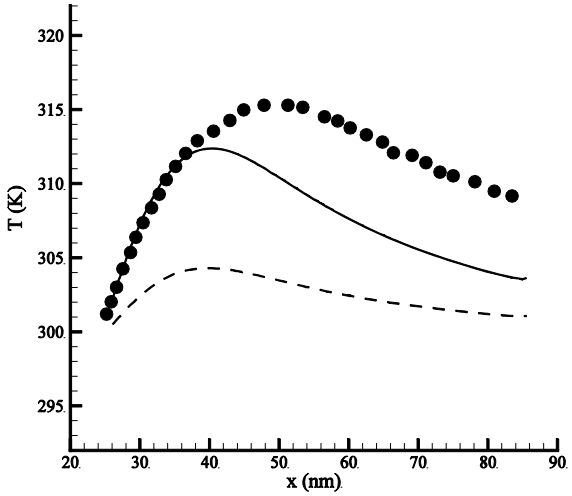

c) T_{in} = 700 K.

Figure 3: Surface gas temperature distribution on wall-3 with various T_{in}.

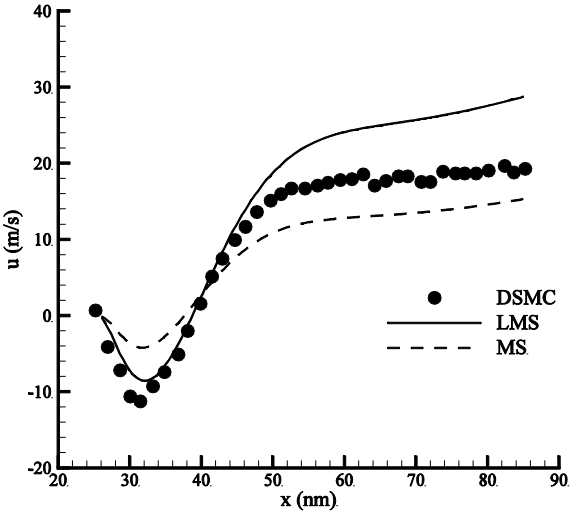

a) T_{in} = 300 K.

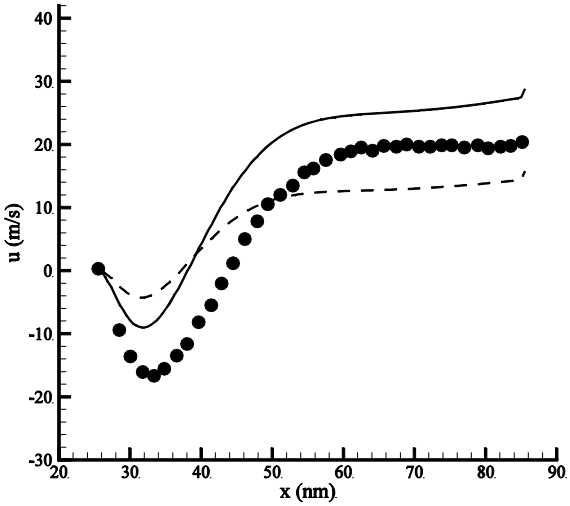

b) T_{in} = 500 K.

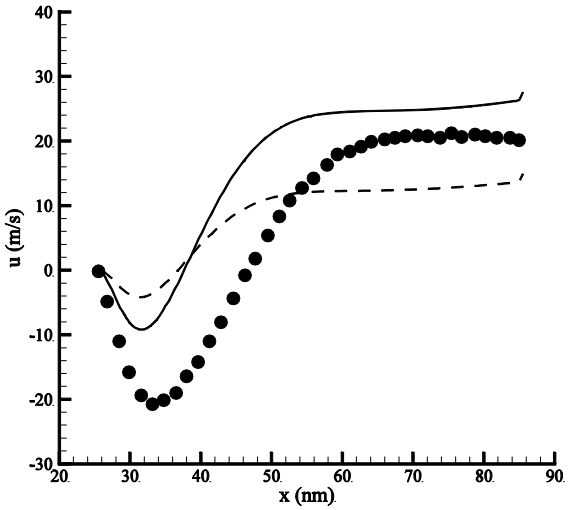

c) T_{in} = 700 K.

Figure 4: Surface gas velocity distribution on the wall-3 with various T_{in}.

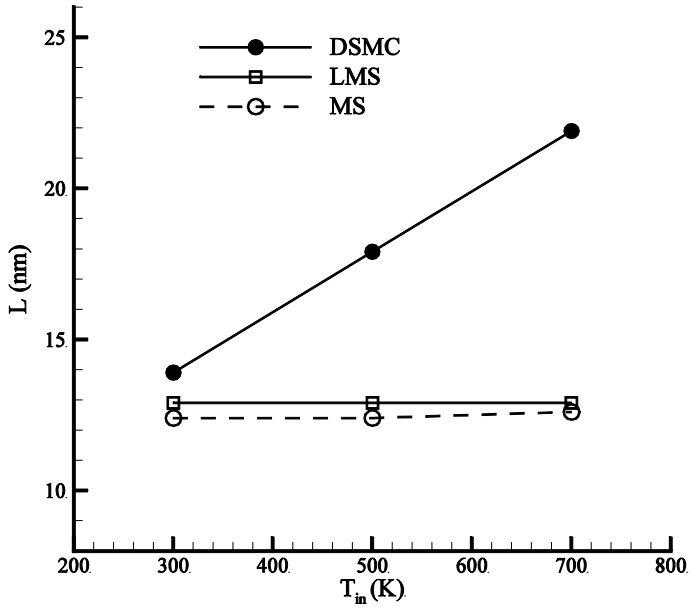

Figure 5: Variation of the separation length with various T_{in}.

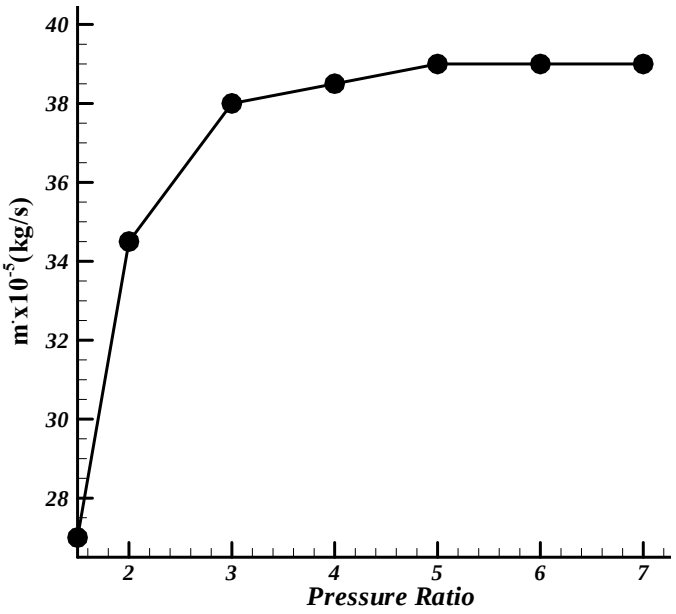

Figure 6: DSMC's mass flow rate variation with various pressure ratios.

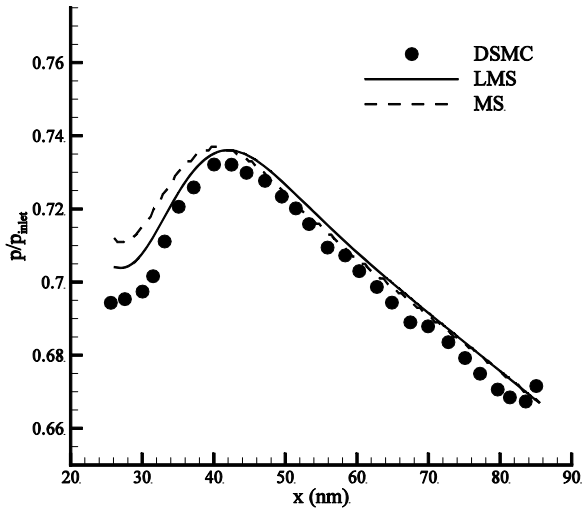

a) PR = 1.5

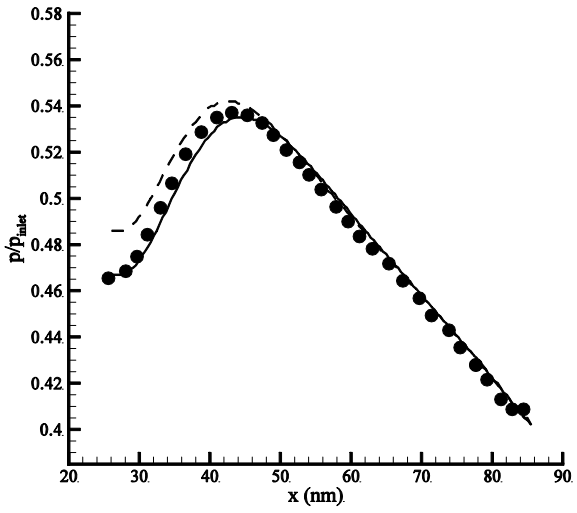

b) PR = 2.5

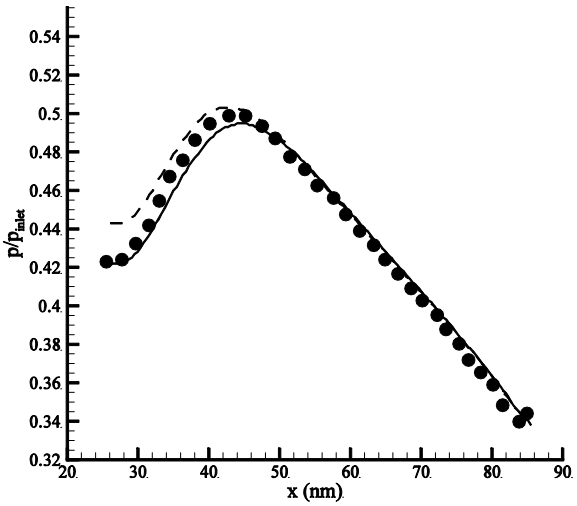

c) PR = 3

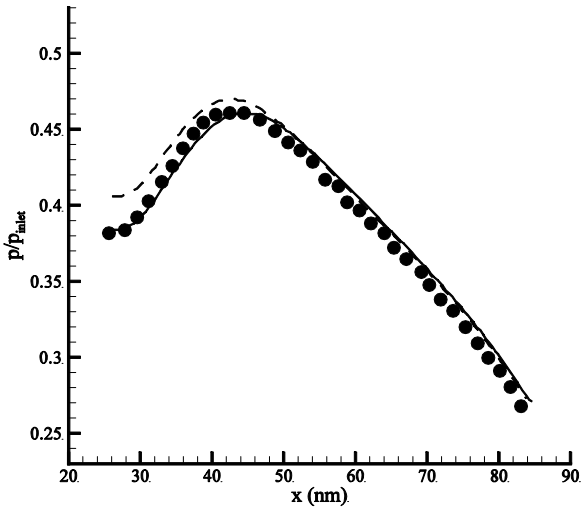

d) PR = 4

Figure 7: Pressure distribution on the wall-3 with various pressure ratios.

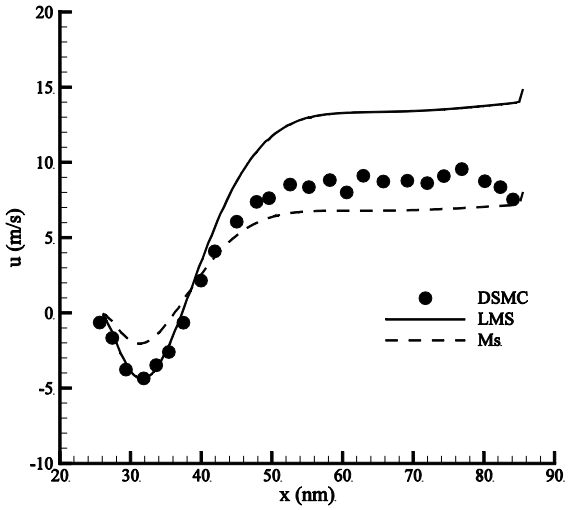

a) PR = 1.5

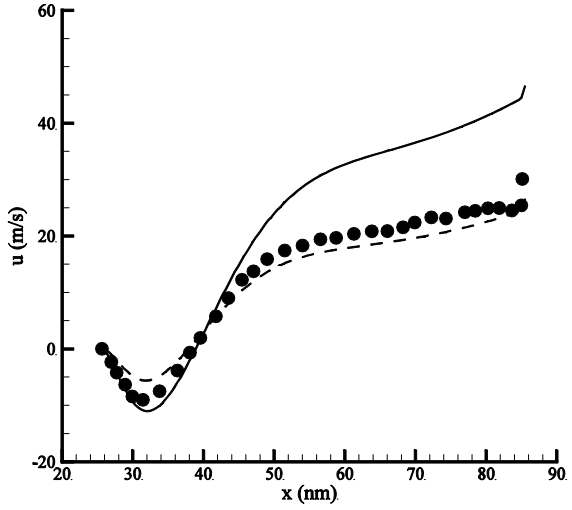

b) PR = 2.5

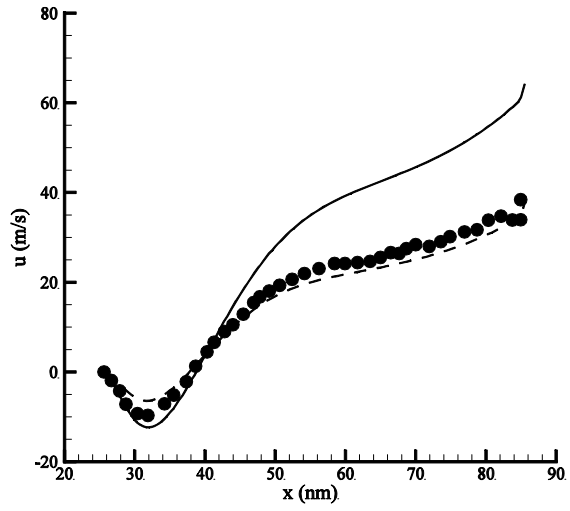

c) PR = 3

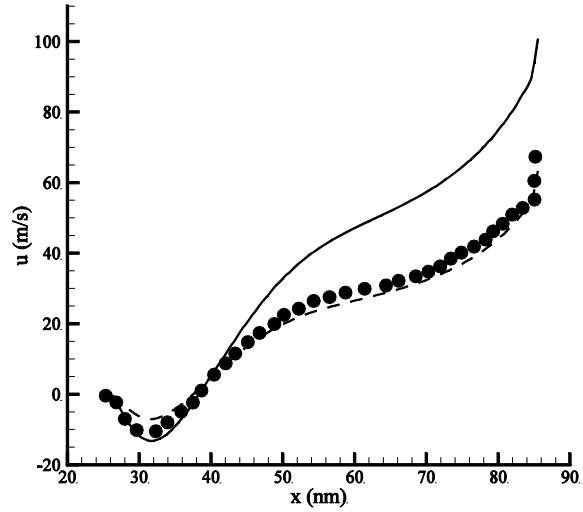

d) PR = 4

Figure 8: Slip velocity distribution on the wall-3 with various pressure ratios.

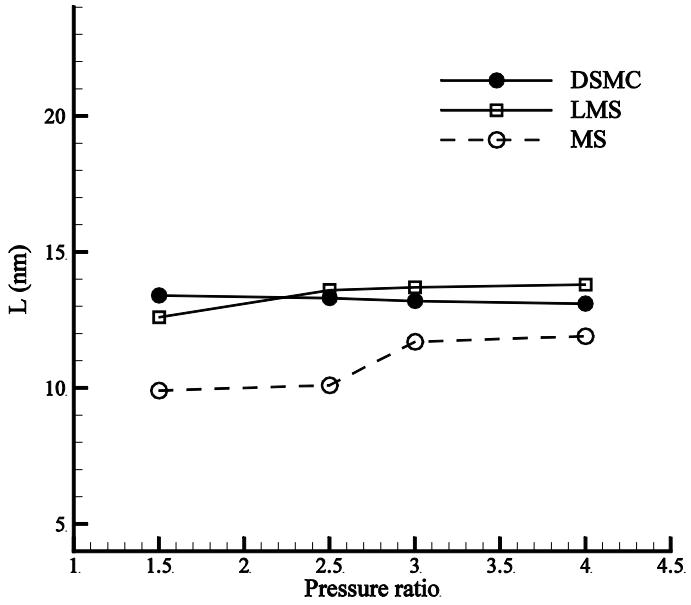

Figure 9: Variation of the separation length with various pressure ratios.

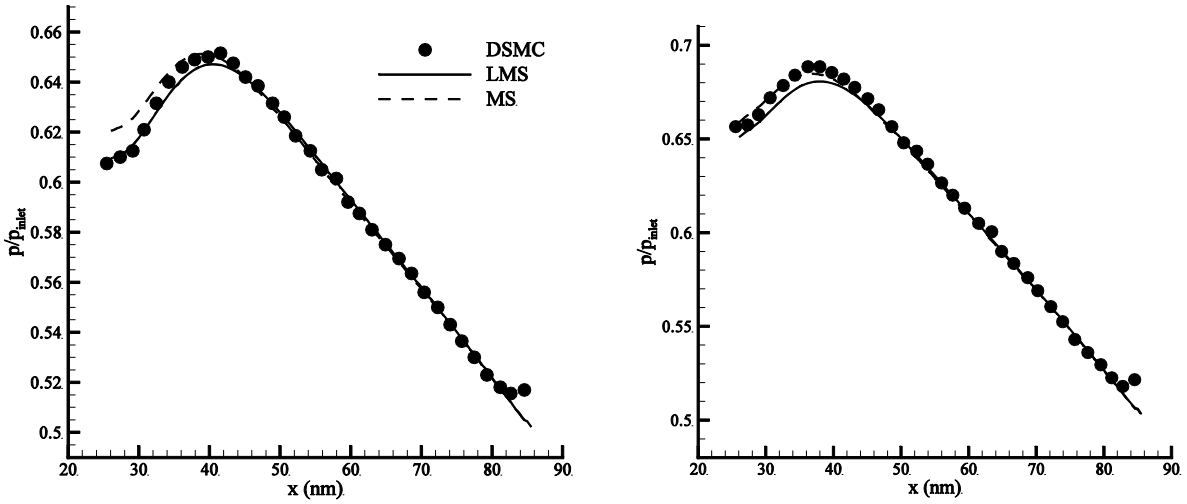

a) T_w = 500 K b) T_w = 700 K

Figure 10: Pressure distribution on the wall-3 with various T_w.

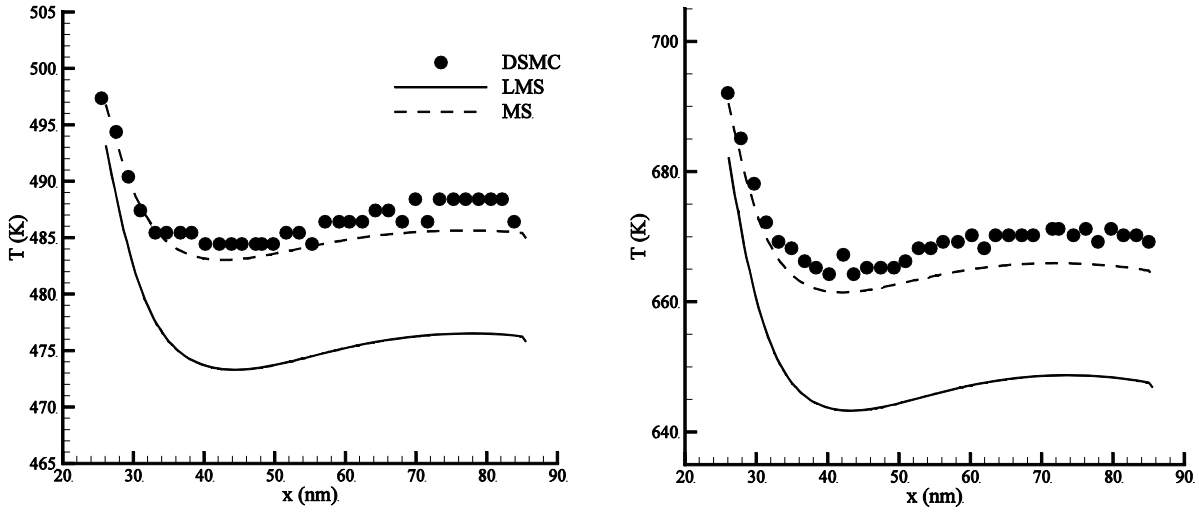

a) T_w = 500 K b) T_w = 700 K

Figure 11: Surface gas temperature distribution on the wall-3 with various T_w.

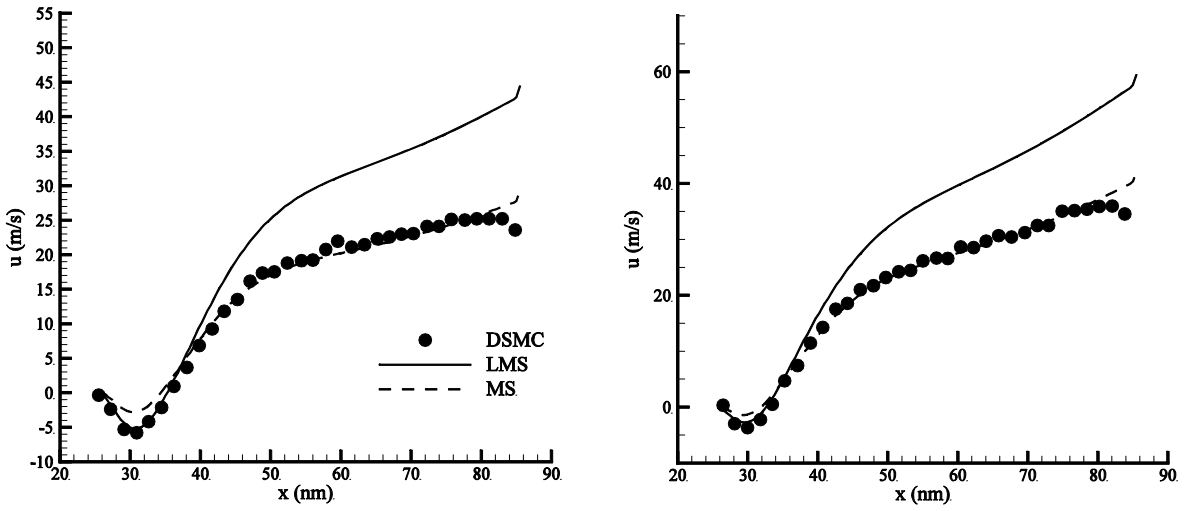

a) T_w = 500 K b) T_w = 700 K

Figure 12: Slip velocity distribution on the wall-3 with various T_w.

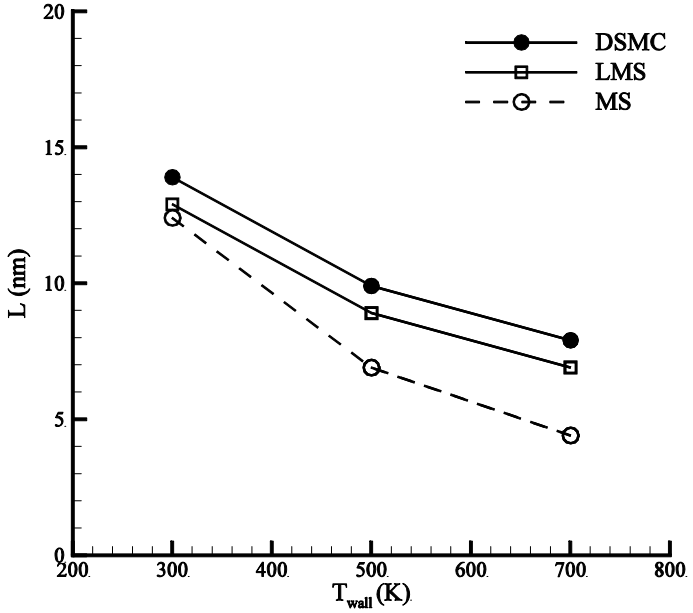

Figure 13: Variation of the separation length with various T_w.

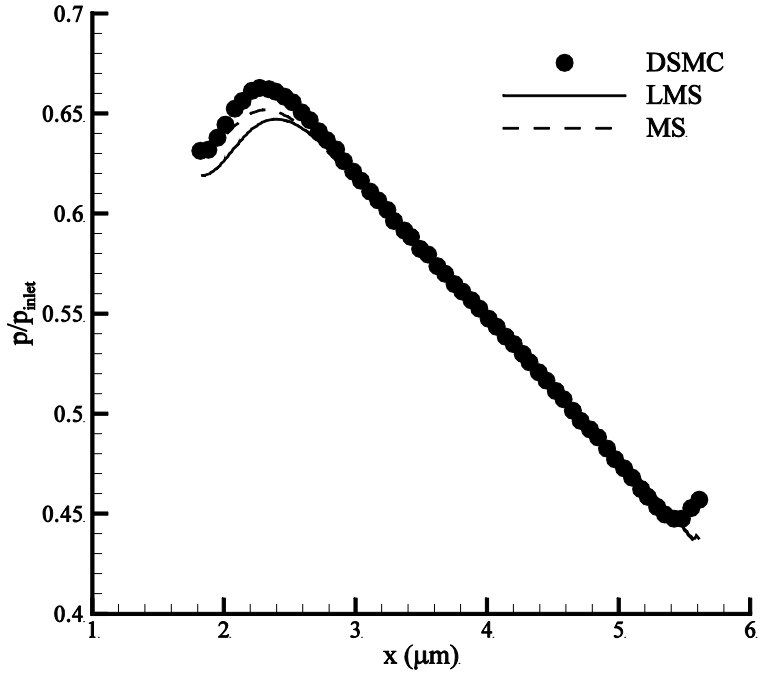

Figure 14: Pressure distribution on the wall-3 of the case $Kn_{in} = 0.05$ (DSMC results are obtained with *dsmcFoamStrath* [20]).

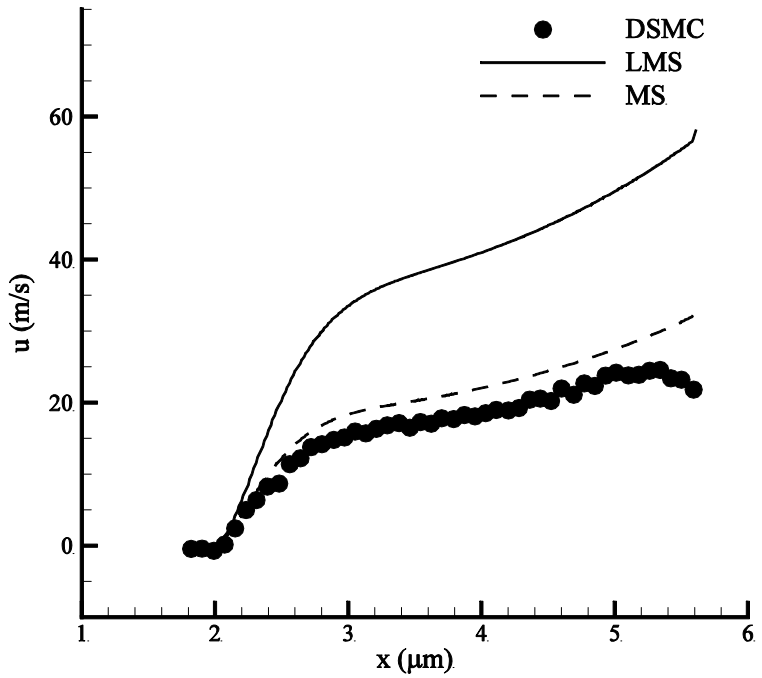

Figure 15: Slip velocity distribution on the wall-3 of the case Kn_{in} = 0.05 (DSMC results are obtained with *dsmcFoamStrath* [20]).

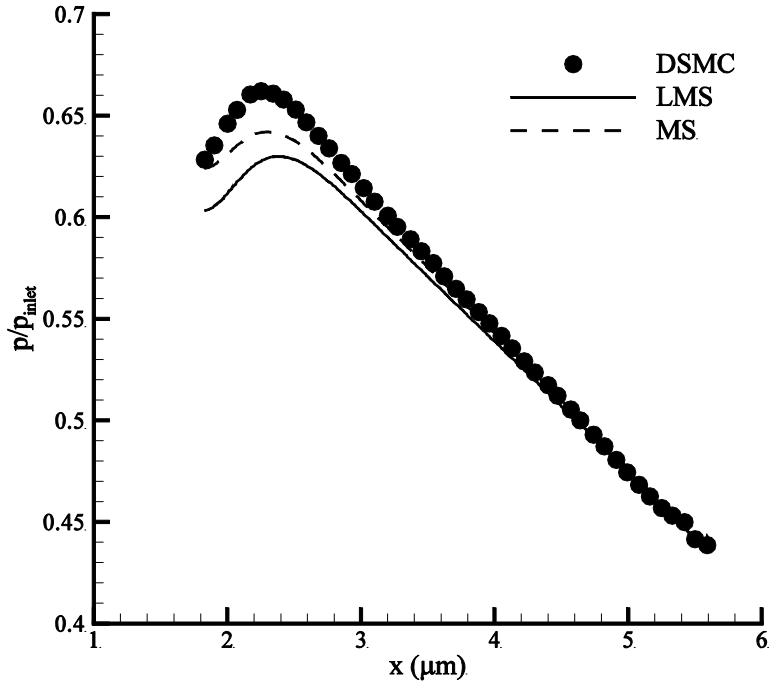

Figure 16: Pressure distribution on the wall-3 of the case Kn_{in} = 0.1 (DSMC results are obtained with *dsmcFoamStrath* [20]).

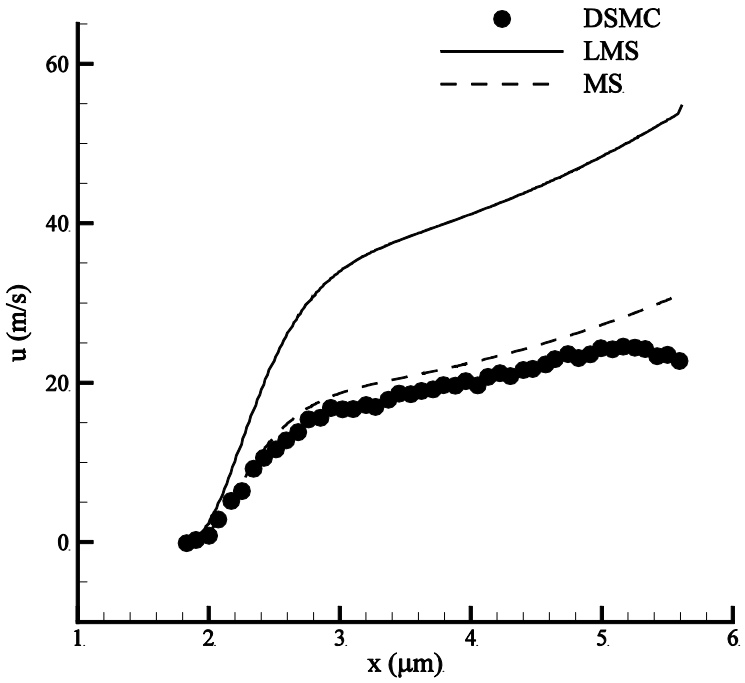

Figure 17: Slip velocity distribution on the wall-3 of the case Kn_{in} = 0.1 (DSMC results obtained with *dsmcFoamStrath* [20]).

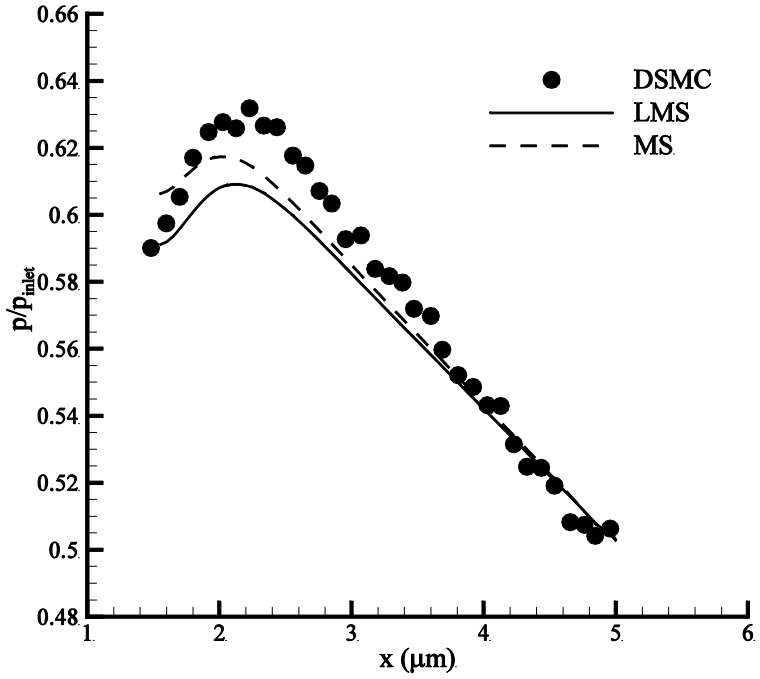

Figure 18: Pressure distribution on the wall-3 of the case Kn_{in} = 0.1 (DSMC results obtained with solver in Ref. [13]).

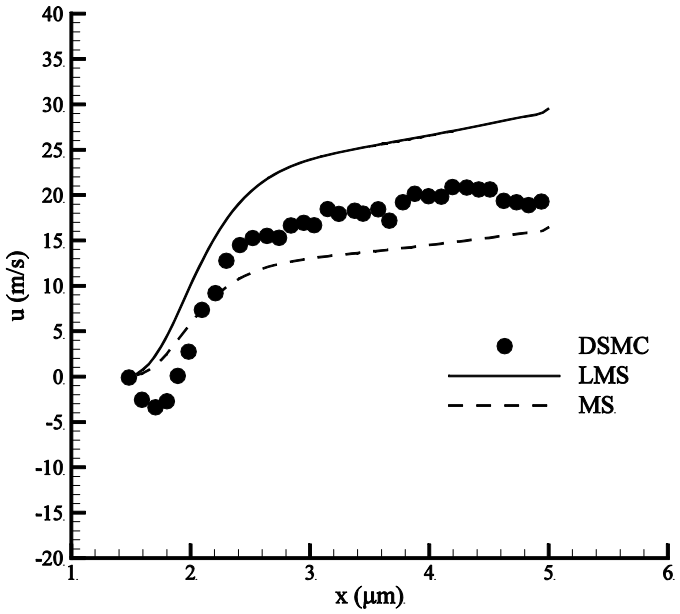

Figure 19: Slip velocity distribution on the wall-3 of the case Kn_{in} = 0.1, (DSMC results obtained with solver in Ref. [13]).